High flexoelectric constants in Janus transition-metal dichalcogenides

Brahmanandam Javvaji[*] and Bo He[*]

Institute of Continuum Mechanics, Leibniz Universität Hannover, Appelstrasse 11, 30167 Hannover, Germany

Xiaoying Zhuang[†]

Institute of Continuum Mechanics, Leibniz Universität Hannover, Appelstrasse 11, 30167 Hannover, Germany
and College of Civil Engineering, Tongji University, 1239 Siping Road, 200092 Shanghai, China

Harold S. Park[†]

Department of Mechanical Engineering, Boston University, Boston, Massachusetts 02215, USA

Due to their combination of mechanical stiffness and flexibility, two-dimensional (2D) materials have received significant interest as potential electromechanical materials. Flexoelectricity is an electromechanical coupling between strain gradient and polarization. Unlike piezoelectricity, which exists only in noncentrosymmetric materials, flexoelectricity theoretically exists in all dielectric materials. However, most work on the electromechanical energy conversion potential of 2D materials has focused on their piezoelectric and not flexoelectric behavior and properties. In the present paper, we demonstrate that the intrinsic structural asymmetry present in monolayer Janus transition-metal dichalcogenides (TMDCs) enables significant flexoelectric properties. We report these flexoelectric properties using a recently developed charge-dipole model that couples with classical molecular dynamics simulations. By employing a prescribed bending deformation, we directly calculate the flexoelectric constants while eliminating the piezoelectric contribution to the polarization. We find that the flexoelectric response of a Janus TMDC is positively correlated to its initial degree of asymmetry, which contributes to stronger σ-σ interactions as the initial degree of asymmetry rises. In addition, the high transfer of charge across atoms in Janus TMDCs leads to larger electric fields due to π-σ coupling. These enhanced σ-σ and π-σ interactions are found to cause the flexoelectric coefficients of the Janus TMDCs to be several times higher than traditional TMDCs, such as MoS_2, whose flexoelectric constant is already ten times larger than graphene.

I. INTRODUCTION

Atomically thin two-dimensional (2D) materials have a variety of unique physical properties that have made them attractive for many different applications [1–11]. An emerging area of interest for 2D materials is electromechanical coupling due to the desire to miniaturize sensors and actuators to the micro- and nanoscales. The most widely studied electromechanical coupling mechanism is piezoelectricity, which has also been investigated for 2D materials, including graphene, hexagonal boron nitride, transition-metal dichalcogenides (TMDCs), and many others [12–24]. We note that the majority of this paper has focused on the in-plane electromechanical properties.

TMDCs exhibit a unique three-layer atomic arrangement where a metallic (M) atom symmetrically bonds with two chalcogenide atoms (X and X) in the out-of-plane direction. This structure makes them good candidates for in-plane stretching-based piezoelectric materials [16], although a recent experimental study measured how an out-of-plane indentation induced an electrical response in MoS_2 [25].

This deformation induced significant changes in the bond lengths between M and X atoms, resulting in a strain gradient, which potentially enabled flexoelectricity, which is a form of electromechanical coupling in which electrical polarization is generated due to strain gradients [17,22,26–29]. Recent work from the present authors [30] investigated the bending flexoelectricity in various 2D materials, including graphene, graphene allotropes, nitrides, graphene analogs of group-IV elements, and TMDCs. That study found that MoS_2 (a MXX material) has a flexoelectric coefficient that is ten times larger than graphene due to enhanced charge transfer resulting from asymmetrical bending-induced changes in the M-X bond lengths.

Because of the impact of asymmetry in the bending-induced changes in the M-X bond lengths in enhancing the flexoelectric properties of MoS_2, we focus here on potential flexoelectric effects in another class of TMDCs, the so-called Janus TMDCs, which introduce an asymmetry in the MXX by replacing one of the X layers of atoms with a different chalcogenide atom Y, resulting in a MXY structure and intriguing physical properties [31–35] as recently reviewed [36]. The changes in the atomic mass and electronic configurations of X and Y atoms in MXY generates an out-of-plane as well as an in-plane dipole moment, which are absent in the MXX structure due to the noncancellation of interactions between

---

[*]These authors contributed equally to this work.

[†]Corresponding authors: zhuang@ikm.uni-hannover.de; parkhs@bu.edu

M-X and M-Y. Density functional theory (DFT) simulations have been used to report high piezoelectric coefficients for various materials in the Janus TMDCs family compared to conventional TMDCs [37], whereas a recent experimental report reported the out-of-plane piezoelectric response for a Janus MoSSe monolayer [38]. Furthermore, multilayer Janus TMDCs have shown very high out-of-plane piezoelectric coefficients due to the increase in vertical dipole moments [37]. Overall, an electromechanical imbalance exists due to the element changes between X and Y in MXY, which should facilitate asymmetric deformation, strain gradients, and, thus, flexoelectricity, whereas also impacting the induced dipole moments in the Janus TMDCs.

Various works have investigated the piezoelectric properties of Janus TMDCs. For example, the tensile load-induced in-plane piezoelectric coefficient (d_{11}) of the Janus TMDCs was found to be several times larger than their out-of-plane shear piezoelectric coefficient (d_{31}) [37,39] where the d_{31} coefficient is absent in most other 2D materials, including MoS$_2$ due to reflection symmetry [16]. Additionally, the out-of-plane piezoelectric coefficient (d_{33}) for monolayer MoSSe under compression was reported to be several orders of magnitude smaller than d_{11} [38]. Under compression, large values for d_{33} were reported for multilayer Janus TMDCs where the monolayers are arranged such that the induced polarization does not cancel out. However, for the multilayer structure, the out-of-plane elastic constants increase with an increasing number of layers, which requires an increasing amount of force to induce deformation in the vertical direction [40] and, thus, is not an optimal choice for electromechanical energy conversion. In contrast, Janus TMDCs as with most atomically thin 2D materials are significantly easier to bend rather than stretch [25,37,41]. The relative ease of bending 2D materials, coupled with the fact that bending intrinsically generates a strain gradient, indicates a significant electromechanical energy conversion potential for bending flexoelectricity as compared to in-plane piezoelectricity for Janus TMDCs.

In order to compare the energy conversion potential between flexoelectricity and piezoelectricity, it is essential to separate the contribution of the flexoelectric response. However, the effect of flexoelectricity is measured in terms of effective piezoelectricity in practice. For example, the experimental work [25] determined the flexoelectric coefficient through a relationship with the measured piezoelectric coefficient under assumptions of small length scales and linear electric fields. An additional example [42] reported the effective out-of-plane piezoelectricity from MoS$_2$. The experimental study reported the piezoelectric responses of a corrugated TMDC [43,44] where electrical polarization is mainly due to the local strain gradients that govern flexoelectricity. A recent study addressed the effective piezoelectricity from the effect of flexoelectricity in a nonpiezoelectric material [45]. Large-scale experimental approaches, such as axial stretching or radial compression of a cylindrical rod wrapped with a nonpiezoelectric material could enable direct measurements of the flexoelectric coefficients [46]. However, experimental methods to find the flexoelectric constants at the nanoscale are unresolved. First-principles simulations can isolate the flexoelectric effect by assuming unstable wrinkles in TMDCs [47]. The authors' previous work [30] provides a mechanical

bending deformation which enables calculation of the flexo-electric response by removing the out-of-plane piezoelectric contribution to the total polarization.

In this paper, we coupled classical molecular dynamics with a charge-dipole (CD) model [48,49] to investigate the bending flexoelectric response of the Janus TMDC family. We first validate the simulation methodology with respect to previous DFT-calculated in-plane piezoelectric coefficients [37]. We then propose a mechanical bending deformation to enable the direct measurement of the flexoelectric response by eliminating the piezoelectric contribution to the polarization. Our results show that the bending flexoelectric constants of Janus TMDCs are significantly higher than that of traditional TMDCs, such as MoS$_2$. The flexoelectric enhancement is found to emerge from the structural asymmetry that is intrinsic to Janus TMDCs, which results in both stronger σ-σ and π-σ interactions than are found in traditional TMDCs.

II. SIMULATION METHOD

We introduce in this section the computational model we use to calculate the electrical polarization due to mechanical deformation. Specifically, a combination of short-range bonded interactions with long-range CD interactions were considered for calculating the forces acting on a given atomic system. According to the CD model [48,49], each atom is assumed to carry a charge q and dipole moment **p**. The short-range atomic interactions are modeled using a Stillinger-Weber potential [50], which was previously used to study the misfit strain-induced buckling for lateral heterostructures with different combinations of TMDCs (MoS$_2$-WSe$_2$, MoS$_2$-WTe$_2$, MoS$_2$-MoSe$_2$, and MoS$_2$-MoTe$_2$). This potential was shown to capture the previously reported spontaneous curling behavior of Janus TMDCs [51]. The CD model requires a parameter R (related to atomic polarizability α) to evaluate the charge and dipole for each atom, which is obtained by matching the calculated polarizability ($\alpha_{\text{Cal.}}$) with the DFT calculated value (α_{DFT}) where the complete details about the process for calculating the CD parameters are given in Ref. [30]. Table I lists the lattice parameters of each Janus TMDC, the parameter R, α_{DFT}, and $\alpha_{\text{Cal.}}$. All the simulations in this paper were conducted in the open-source molecular dynamics code LAMMPS [57]. The GAUSSIAN software [58] was employed to estimate α_{DFT}. The details of the atomic forces resulting from the CD model can be found in Ref. [22] and references therein.

The current DFT calculations do not consider spin-orbit coupling (SOC). We tabulated the spontaneous dipole moment for Janus TMDCs from the present CD model ($p_{\text{Cal.}}^0$) and recent DFT reports with and without SOC (p_{DFT}^0). While SOC does have some effect on the results, Table I shows that the comparison between $p_{\text{Cal.}}^0$ and p_{DFT}^0 is quite satisfactory. This shows that the present CD model is sufficiently accurate to predict the flexoelectric properties.

We first validated the CD model by comparing to previously reported in-plane piezocoefficients [37]. In this paper, the in-plane piezoelectric coefficients of the Janus TMDCs (MXY, where $M =$ Mo, W; $X, Y =$ S, Se, and Te where the atomic mass of X is smaller than the atomic mass of Y) are obtained by subjecting a square Janus TMDC sample with

TABLE I. The spontaneous dipole moment from the present CD model ($p^0_{\text{Cal.}}$ in eÅ) and recent DFT reports with and without SOC (p^0_{DFT} in eÅ). Total polarizability estimated by DFT (α_{DFT} in Å^3) and the present CD model ($\alpha_{\text{Cal.}}$ in Å^3) [30]. Atomic polarizability (R_i in angstroms) and lattice parameters (a and b are the lattice constants, l_1 and l_2 are the bond lengths for M-X and M-Y in angstroms, respectively) for the Janus TMDCs. For simplicity, in this paper, the Janus TMDCs are denoted as MXY with $M =$ Mo and W; $X, Y =$ S, Se, and Te; X represents the chalcogenide atom with smaller atomic number whereas Y represents the chalcogenide atom with a larger atomic number.

Material	$p^0_{\text{Cal.}}$	p^0_{DFT}	α_{DFT}	$\alpha_{\text{Cal.}}$	R_M	R_X	R_Y	a, b	l_1	l_2
MoS$_2$	0.0	0.0[a]	12.320	12.350	0.69	1.04	1.04	3.160[b]	2.420[b]	2.420[b]
MoSSe	0.032	0.0391,[c,d] 0.052[e,f]	13.456	13.450	0.84	1.14	1.06	3.288[b]	2.416[b]	2.530[b]
MoSTe	0.0432	0.0412[c]	15.590	15.593	1.0	1.16	1.02	3.343[b]	2.432[b]	2.715[b]
MoSeTe	0.0649	0.079[c]	16.768	16.769	1.04	1.12	1.05	3.412[b]	2.552[b]	2.717[b]
WSSe	0.0479	0.0362,[c] 0.05[e]	16.824	16.822	0.94	1.18	1.08	3.232[b]	2.421[b]	2.538[b]
WSTe	0.0574	0.0389[c]	19.489	19.489	1.08	1.18	1.08	3.344[b]	2.438[b]	2.720[b]
WSeTe	0.0587	0.0757[c]	21.225	21.224	1.08	1.24	1.08	3.413[b]	2.559[b]	2.722[b]

[a]Reference with SOC [52].
[b]Reference [53].
[c]Reference with SOC [54].
[d]Reference without SOC [33].
[e]Reference with SOC [55].
[f]Reference without SOC [56].

dimensions 80×80 Å^2 to tensile loading in the y direction as shown in Fig. 1(a). The initial configuration is flat, and the relaxed atomic configurations of the Janus TMDC are

obtained through energy minimization after which the atomic charge q_i and dipole moments $\mathbf{p}_i$ are derived from the CD model for atom i. The relaxed configuration is bent due to
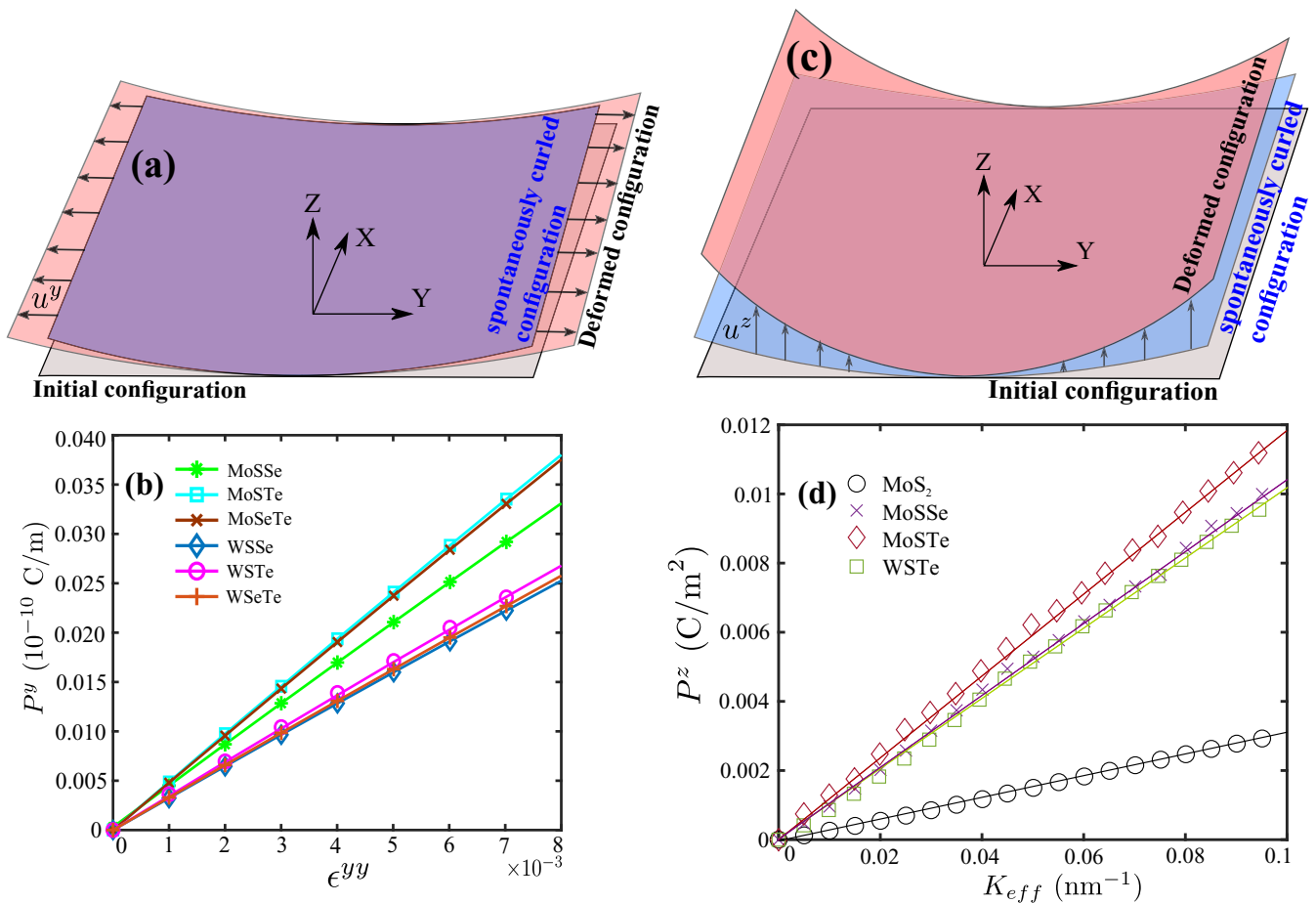

FIG. 1. (a) Loading scheme for calculating the in-plane piezoelectric coefficient d_{11} and (b) polarization P^y (C/m) vs strain ϵ^{yy} for the Janus TMDC systems. (c) Schematic of applied bending deformation to calculate the flexoelectric constants. (d) Polarization P^z (C/m^2) vs strain gradient K_{eff} (nm^{-1}) for MoS$_2$, MoSSe, MoSTe, and WSTe. The markers indicate the data from the CD model, and the solid lines indicate the linear fitting.

TABLE II. In-plane piezoelectric coefficients $d_{yyy}(\times 10^{-10}$ C/m) for Janus TMDCs using the proposed CD model in comparison to previous DFT results (d_{yyy}^{DFT}). μ_{zyzy} (nC/m)'s are the bending flexoelectric constants whereas $l_2 - l_1$ (Å) is the initial asymmetry for Janus TMDCs.

Material	d_{yyy}	d_{yyy}^{DFT}	$l_2 - l_1$	μ_{zyzy}
MoS_2	3.95	3.56[a]	0.0	0.032
MoSSe	4.099	3.74[a]	0.114	0.117
MoSeTe	4.676	4.35[a]	0.165	0.120
MoSTe	4.733	4.53[a]	0.283	0.125
WSSe	3.144	2.57[a]	0.117	0.089
WSeTe	3.209	3.34[a]	0.163	0.092
WSTe	3.327	3.48[a]	0.282	0.114

[a]Reference [37].

spontaneous curling [31,51], which arises from the structural asymmetry between the M-X and M-Y layers, resulting in stretching in the Y layer and compression in the X layer.

The total polarization **P** of the system is calculated by $\mathbf{P} = \frac{1}{V}(\sum_{i=1}^{n} \mathbf{p}_i)$ where V is the volume and n is the total number of atoms in the system. The in-plane strain is calculated by $\epsilon^{yy} = \frac{ly - ly_{\text{ini}}}{ly_{\text{ini}}}$, where ly and ly_{ini} are the deformed length and initial length in the y direction, respectively. The loading scheme for calculating the in-plane piezoelectric coefficient and polarization (P^y)-strain (ϵ^{yy}) diagrams are presented in Figs. 1(a) and 1(b). The polarization (P^y)-strain (ϵ^{yy}) diagrams are shifted to have zero initial polarization by subtracting the polarization caused by the initial spontaneous curling [51]. A linear relation is observed between the polarization P^y and the given strain ϵ^{yy} in Fig. 1(b). The slope of the linear relation yields the in-plane piezoelectric coefficient of the Janus TMDCs. The calculated piezoelectric coefficients (d_{yyy} or d_{11}) are in good agreement with the reported DFT values [37] (see Table II), which validates the effectiveness of the CD model.

III. RESULTS AND DISCUSSION

In this section, we describe the bending scheme used to study the flexoelectric properties of Janus TMDCs. To determine the bending flexoelectric coefficients for the Janus TMDCs, the loading scheme illustrated in Fig. 1(c) is applied. Specifically, the following displacement field is applied to the atomic system:

$$u^z = K\frac{y^2}{2},\tag{1}$$

where y represents the atom coordinate in the y direction and $\frac{1}{2}K$ represents the given strain gradient of the bending plane. We note that the imposed displacement field in Eq. (1) is imposed starting from the relaxed, or spontaneously curved, configuration in Fig. 1(c). Once the deformation is prescribed, the boundary region atoms are held fixed whereas the interior atoms are allowed to relax to energy minimizing positions using the conjugate-gradient algorithm after which the point charges q_i and dipole moments $\mathbf{p}_i$ are found for each atom by the CD model. The bending flexoelectric constant μ_{zyzy} can
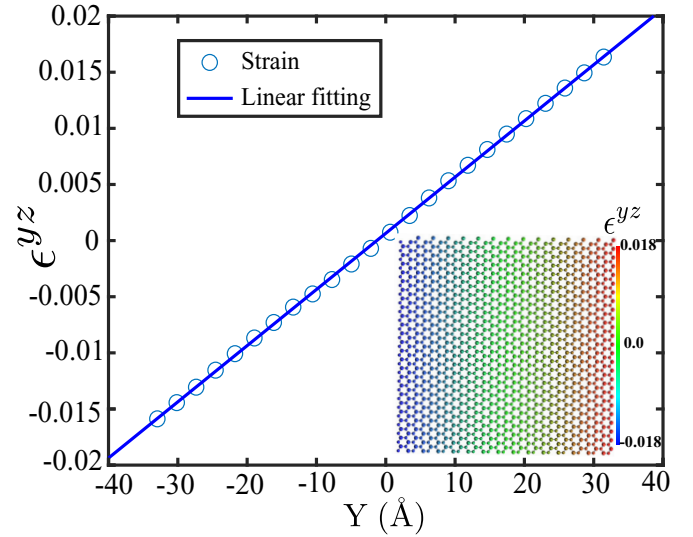

FIG. 2. Strain profile ϵ_{yz} vs y coordinates Y. The inset shows a contour plot of the strain ϵ_{yz}.

then be obtained as the slope of the resulting plot between polarization and strain gradient.

In general, an imposed deformation would induce polarization, which has contributions from both piezoelectric and flexoelectric effects. The current bending deformation in Eq. (1) induces only the strain component ϵ^{yz} and the strain gradient term ($\frac{\partial \epsilon^{yz}}{\partial y}$), whereas the remaining components of the strain and strain gradient tensors are zero. Therefore, the total induced polarization in the z direction is

$$P^z = d_{zyz}\epsilon^{yz} + \mu_{zyzy}\frac{\partial \epsilon^{yz}}{\partial y},\tag{2}$$

where d_{zyz} and μ_{zyzy} are the bending piezoelectric coefficient and flexoelectric coefficient, respectively. The inset of Fig. 2 represents the atomic configuration of MoSSe obtained using the OVITO software [59] when the applied curvature $K = 0.05$ nm^{-1}. The atoms are colored according to the ϵ^{yz} component of strain, which is calculated from Eq. (3) as [60,61]

$$\epsilon_i^{\alpha\beta} = \frac{1}{2}\big[F_i^{\beta\alpha}F_i^{\alpha\beta} - \delta^{\alpha\beta}\big],\tag{3}$$

where ϵ_i is the atomic strain for atom i, $F_i^{\alpha\beta}$ is the ith atomic component of the deformation gradient, δ is the Kronecker δ, and α and β are the coordinate components.

As shown in Fig. 2, the strain ϵ^{yz} varies from -0.018 to 0.018 along the y direction in the MoSSe sheet. These strain values represent averaged values of the atomic strain, which were found by averaging over 24 equal-width bins along the y direction. The linear variation of atomic strain indicates that total strain is zero and maintains the point-group symmetry posed by MXY [37]. Overall, the observed symmetry removes the piezoelectric part of polarization $d_{zyz}\epsilon^{yz} = 0$, which supports the assumption that the imposed bending deformation removes the piezoelectric contribution to the polarization.

The slope of the plot in Fig. 2 between ϵ^{yz} and the y coordinate of each bin leads to the effective strain gradient $K_{\text{eff}} = \partial\epsilon^{yz}/\partial y$. The current value of K_{eff} differs from $\frac{1}{2}K$ [from Eq. (1)] by about 15%. Theoretically, the numerical value of K_{eff} should be equal to $\frac{1}{2}K$ under the imposed bending deformation. For example, previous works found that, for
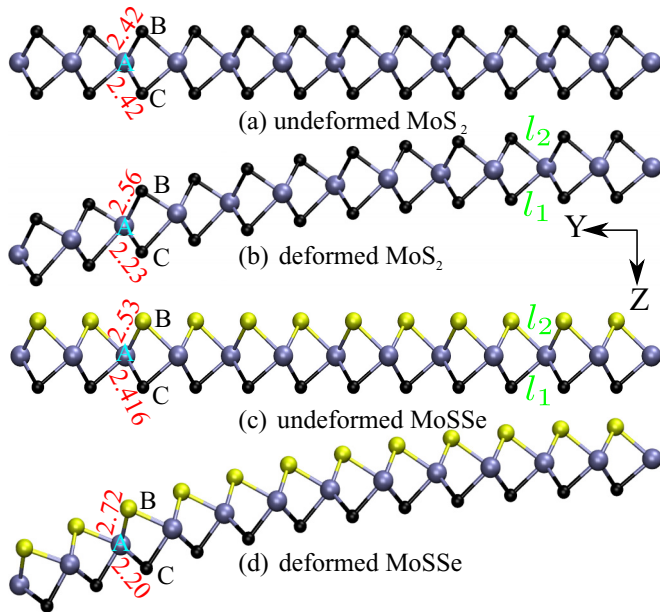
FIG. 3. Atomic configurations of (a) undeformed MoS_2, (b) deformed MoS_2 at $K_{eff} = 0.05$ nm^{-1}, (c) undeformed MoSSe, and (d) deformed MoSSe at $K_{eff} = 0.05$ nm^{-1}.

conventional TMDCs (MoS_2, WS_2 and CrS_2), the effective strain gradient is equal to half of the given value of K [30] under the same bending deformation. However, the observed difference in Janus TMDCs is due to the spontaneous curling effect [31,51], which arises from the structural asymmetry between the M-X and the M-Y layers, resulting in stretching in the Y layer and compression in the X layer. In order to account for the spontaneous deformation, the effective strain gradient K_{eff} is used in our calculations of the flexoelectric coefficient.

We note that a similar type of curling, i.e., ripplocations, has been observed in MoS_2 by introducing line defects (the removal of sulfur atoms along a line) [62], which generate local strain gradients and, thus, flexoelectricity. However, in the present paper, we restrict ourselves to calculations of intrinsic flexoelectricity for spontaneously curled Janus TMDCs.

A. Flexoelectric effect in MoS_2 and MoSSe

In this section, we examine MoS_2 and MoSSe to illustrate the effects of structural asymmetry on the resulting flexoelectric properties. MoS_2 is chosen as a TMDC that does not have structural asymmetry (MXX), whereas MoSSe is chosen as a representative Janus TMDC which does have structural asymmetry (MXY). To aid in the analysis of the resulting flexoelectric constants, we note that the dipole moment of an atom **p** depends primarily on three factors: the effective atomic polarizability (R), the charge-induced electric-field (E^{q-z}), and the dipole-induced electric-field (E^{p-z}). We focus as shown previously in Eq. (2) on the out-of-plane (z-direction) dipole moment p^z and associated polarization P^z.

The bond length between atoms A-B and A-C in Fig. 3(a) is equal to 2.42 Å (l_{Mo-S}) for unbent MoS_2. Because the A-B and A-C bond lengths are the same, there is no initial structural asymmetry for MoS_2, and the bonds induce equal and

opposite electric fields, which cause the total dipole moment and, thus, total polarization of each MoS_2 unit cell to be zero. However, significant changes in the bond lengths are observed in the deformed state [Fig. 3(b)] for a curvature of $K_{eff} = 0.05$ nm^{-1}. Bond A-B is stretched from 2.42 to 2.56 Å whereas bond A-C is compressed from 2.42 to 2.23 Å. This difference in bond lengths breaks the electric-field symmetry and increases the total dipole moment. At $K_{eff} = 0.05$ nm^{-1}, the total electric-field difference $\Delta(E^{p-z} + E^{q-z})$ with respect to the initial (undeformed) configuration is 53.06 V/Å, which increases the total polarization from 0 to 0.0016 C/m^2. The changes to E^{q-z} and E^{p-z} at $K_{eff} = 0.05$ nm^{-1} are 45.6 and 7.4 V/Å, respectively. The significant contribution of E^{q-z} implies the increasing importance of π-σ interactions in generating the dipole moment p^z. The π-σ interactions originate from the coupling between valence electrons and bonding electrons [63], which are also interpreted as pyramidalization [29,64,65]. Furthermore, a recent DFT study reported [66] electron transfer from the p orbitals of S atoms to the d_{z^2} orbitals of Mo atoms. This electron transfer modifies the charges on the Mo and S atoms, which generates local charge-induced electric fields, which are captured through E^{q-z} within the current CD model. Further changes in the bond length between Mo and S atoms enhance the π-σ coupling [35], resulting in large E^{q-z} and P^z. The variation of total polarization with the effective strain gradient for MoS_2 is given in Fig. 1(d) where the slope represents the flexoelectric constant for MoS_2 (μ_{MoS_2}), which is found to be 0.032 nC/m.

In contrast to MoS_2, the Janus TMDC MoSSe has a structural asymmetry in the undeformed configuration between the Mo-S and the Mo-Se atomic layers. Specifically, the A-B (l_{Mo-Se}) bond length in Fig. 3(c) is equal to 2.53 Å, whereas the A-C bond length (l_{Mo-Se}) is 2.416 Å. The bending deformation of MoSSe to a curvature of $K_{eff} = 0.05$ nm^{-1} stretches $l_{Mo-Se}(l_2)$ from 2.53 to 2.72 Å and shrinks $l_{Mo-S}(l_1)$ from 2.416 to 2.20 Å. The initial bond length asymmetry in MoSSe is further increased due to the given deformation and helps to produce larger dipole moments p^z, compared to MoS_2. The dipole moment p^z is also related to the polarizability of the atomic system where the polarizability of MoSSe (α_{MoSSe}) is 1.09 times larger than that of MoS_2 (α_{MoS_2}) as shown in Table. I, which shows the important effect of structural asymmetry for the Janus TMDCs.

In addition, the initial bond length asymmetry in unbent MoSSe induces an intrinsic electric field, which is not present in MoS_2 as shown in recent DFT simulations [33]. That work also reported the nonoverlapping of out-of-plane wave functions for electrons and holes due to this electric field, which implies a weak bonding between the electron-hole pair and which reduces the band gap by pushing the d orbitals of the metal atom closer to the Fermi level [67]. The d-orbital shifting may enhance the charge-transfer process through π-σ coupling, which represents an easy transfer of charges from the S or Se atom to the Mo atom. This phenomenon is reflected in our CD model as the calculated charge on Mo [atom A in Fig. 3(d)] in MoSSe is $0.733e$, which is significantly larger than for Mo in MoS_2 [atom A in Fig. 3(b)], which is $0.282e$, and, as such, the charge acquired by the Mo atom in MoSSe is 2.6 times higher than in MoS_2.

For a curvature of $K_{\mathrm{eff}} = 0.05 \; \mathrm{nm}^{-1}$, the charge-transfer-induced change in E^{q-z} in MoSSe is 117.6 V/Å, which is exactly 2.6 times higher than the field induced in MoS$_2$, and which reflects stronger π-σ coupling in MoSSe. Furthermore, the value of E^{p-z} is higher in MoSSe (38.4 V/Å) than in MoS$_2$ (7.4 V/Å), which represents a stronger dipole interaction (σ-σ coupling) in MoSSe than MoS$_2$. Recent studies on the electronic properties of strained Janus TMDCs [35] suggest an increased coupling between the p orbitals of S/Se atoms with the in-plane bonding orbitals $d_{x^2-y^2}$ and d_{xy} of the Mo atom as a function of changes in bond angle. In MoSSe, the angle B-A-C in Fig. 3 varies from 81.1° to 74.2° between the initial and the deformed states ($K_{\mathrm{eff}} = 0.05 \; \mathrm{nm}^{-1}$), whereas for MoS$_2$, angle variations are 81.93° to 78.66° for the initial and deformed states. The reduction in bond angles between MoSSe and MoS$_2$ may increase the contribution of E^{p-z} in MoSSe.

Overall, E^{q-z} is higher than E^{p-z} in MoSSe, which represents that π-σ coupling is dominant over σ-σ coupling. DFT simulations have shown that coupling between d_{z^2} and p orbitals (π-σ coupling) is stronger than the coupling among p and $d_{x^2-y^2}$ and d_{xy} (σ-σ coupling) orbitals [35,67] in Janus TMDCs. The total electric-field increment $\Delta(E^{p-z} + E^{q-z})$ in MoSSe is 156.07 V/Å at a curvature of $K_{\mathrm{eff}} = 0.05 \; \mathrm{nm}^{-1}$, which is 2.94 times higher than in MoS$_2$ at the same curvature. The increased polarizability and electric field increase the total dipole moment of MoSSe to 3.24 times higher than in MoS$_2$. The flexoelectric constant for MoSSe (μ_{MoSSe}) is found to be 0.117 nC/m, which is 3.6 times higher than the flexoelectric coefficient of MoS$_2$, which is consistent with the larger polarizability of MoSSe. The polarizability is directly related to the dielectric constant (ε) of the material [68]. For instance, α of MoSSe and MoS$_2$ are 13.45 and 12.35 Å^3, respectively, as shown in Table I. The DFT-calculated values for ε for these materials are 8.67 and 8.05 [33]. Thus, the increased flexoelectric constant for MoSSe over MoS$_2$ is in agreement with the fact that flexoelectric effect scales with the material dielectric constant [69,70].

As previously shown in Table II, the in-plane piezoelectric coefficient for MoSSe is comparable with that of MoS$_2$. However, the out-of-plane flexoelectric coefficient is 3.6 times higher than MoS$_2$ (Table II), which implies that there are relative benefits to bending flexoelectricity as compared to in-plane piezoelectricity when comparing Janus TMDCs to standard TMDCs. In order to understand this further, we compare the change in total electric field and asymmetry in bond length between in-plane tensile deformation and out-of-plane bending deformation for MoSSe for the same strain energy density, which is defined as the sum of atomic stress times the atomic strain over the volume of the deformed system. The changes in E^{q-z} and E^{p-z} for bending deformation were previously noted as 117.6 and 38.4 V/Å for a curvature of $K_{\mathrm{eff}} = 0.05 \; \mathrm{nm}^{-1}$, whereas, for tensile deformation, the values are 11.9 and 18.7 V/Å, respectively. This shows that the induced electric fields are higher in bending than in tension, which generates high dipole moments. It is also observed that the difference in bond length ($l_2 - l_1$) for bending is higher than in tension for the same unit cell compared in tension and bending. This reflects the larger bond length asymmetry that

is induced in bending, which supports the charge transfer and enhanced π-σ coupling-based electric fields.

To further compare the resulting electromechanical coupling between standard TMDCs and Janus TMDCs, we have computed the electrical energy density for atomic configurations at the same strain energy density for MoSSe and MoS$_2$. The electrical energy density is defined as the sum of the dot product between induced polarization and electric field over the volume. The atomic configuration of MoSSe at $K_{\mathrm{eff}} = 0.05 \; \mathrm{nm}^{-1}$ gives an electrical energy density of $2.6 \times 10^9 \; \mathrm{J/m^3}$ and a strain energy density of $1.13 \times 10^9 \; \mathrm{J/m^3}$. By selecting an atomic configuration for MoS$_2$ under bending deformation with the same strain energy density results in an electrical energy density that is about 39% of the MoSSe electrical energy density. The electrical energy density under tensile deformation of MoSSe is about 84% of the electrical energy density for MoSSe under bending. These results show that the higher values of electric fields and large dipole moments under the bending deformation point to the advantage of bending as compared to stretching in generating strong electromechanical coupling in Janus TMDCs.

B. Flexoelectric effect among Janus TMDCs

From the previous section, it is clear that the asymmetry in bond lengths between layers of MXY induce large dipole moments through the increase in induced electric fields. Table II lists the out-of-plane bending flexoelectric coefficients of the Janus TMDCs along with the initial bond length difference $l_2 - l_1$ in Fig. 3 from which a positive correlation is identified for both the MoXY and the WXY Janus TMDCs. We note that the out-of-plane piezoelectric coefficients also show a similar dependence on bond length asymmetry [37]. We mechanistically examine this correlation further using the electric fields due to charge-dipole (E^{q-z}) and dipole-dipole (E^{p-z}) interactions from the CD model.

Under the prescribed bending scheme, the increase in the total electric-field $E^{q-z} + E^{p-z}$ increases with strain gradient K_{eff} for every Janus TMDC. However, the relative contribution from E^{q-z} or E^{p-z} to $E^{q-z} + E^{p-z}$ varies between elements of the Janus TMDCs group. In the MoXY group, for a strain gradient of $K_{\mathrm{eff}} = 0.1 \; \mathrm{nm}^{-1}$, the contribution from the charge-dipole interaction-induced electric-field E^{q-z} in MoS$_2$, MoSSe, MoSeTe, and MoSTe to the increase in the total electric-field ($E^{q-z} + E^{p-z}$) is 84.76%, 75.48%, 70.33%, and 56.29%, respectively. The contribution from the dipole-dipole interaction-induced electric-field E^{p-z} to the increase in the total electric-field ($E^{q-z} + E^{p-z}$) is then 15.24%, 24.52%, 29.67%, and 43.71% in MoS$_2$, MoSSe, MoSeTe, and MoSTe, respectively.

The bending deformation further develops a coupling among the induced dipole moments via the σ-σ interactions, which raises the contribution of E^{p-z}. For example, in MoSTe, at $K_{\mathrm{eff}} = 0.01 \; \mathrm{nm}^{-1}$, E^{q-z} and E^{p-z} are 56.82 and 33.99 (V/Å), respectively. When K_{eff} is increased to $0.05 \; \mathrm{nm}^{-1}$, these values increase to 280.5 and 216.99 (V/Å). The enhanced dipole-dipole interaction E^{p-z} is due to the reduction in bond angle via the increased bond length asymmetry due to bending. The decrease in bond angle (B-A-C in Fig. 3) between initial and deformed states ($K_{\mathrm{eff}} = $

0.05 nm^{-1}) is $6.9°$ for MoSSe and $7.4°$ for MoSTe. The difference in E^{p-z} for atom A in MoSSe is 0.38 V/Å and for atom A in MoSTe is 0.53 V/Å (not shown in Fig. 3). This further confirms that the increased reduction in the bond angle helps in increasing the dipolar interactions (σ-σ coupling), which are measured in the form of E^{p-z}. Note that atoms A, B, and C are selected at exactly the same unit-cell locations in MoSSe and MoSTe. The cumulative effect of bond angle reduction within the unit cell and across the unit cell in the given atomic system makes the contribution of E^{p-z} significant. The total effect of increased electric fields and polarizability helps in inducing high polarization and, thus, the high flexoelectric coefficient for MoSTe over other Janus TMDCs. A similar trend is found in the WXY group in Table II where high charge transfer and higher bond angle reduction in WSTe compared to other elements in the WXY group. This makes the flexoelectric coefficient of WSTe higher than WSSe and WSeTe.

Table II also shows that the MoXY group exhibits higher out-of-plane bending flexoelectric coefficients than the WXY group. For example, MoSTe and WSTe have the highest flexoelectric coefficients in their groups where the flexoelectric coefficient of MoSTe is about 1.09 times larger than WSTe. At $K_{\text{eff}} = 0.05$ nm^{-1}, the total electric-field change in MoSTe is found to be 1.4 times larger than that of WSTe while the polarizability of MoSTe is 0.79 times that of WSTe. Although the polarizability of MoSTe is lower than WSTe, the larger induced electric fields result in the flexoelectric constant of MoSTe being slightly larger than that of WSTe.

C. Bending against the initial spontaneous curvature

Up to this point, we have studied the bending-induced flexoelectric response of MXY materials while applying the out-of-plane bending toward to their initial curling direction (towards S in the case of MoSTe). In this section, we apply bending deformation against the initial curling direction (towards Te in the case of MoSTe) to study the effect of the bending direction on the induced polarization. We followed the same simulation procedure described in Sec. II except for inserting a minus sign in Eq. (1) to indicate that the applied deformation is opposite to the initial curling direction.

Figure 4 shows the variation of P^z with K_{eff}. The dashed line at $K_{\text{eff}} = K_{\text{flat}}$ represents the flattening of the MoSTe sheet from the initial spontaneously curved state. The notable feature of Fig. 4 is that the total polarization P^z increases up to K_{flat} and decreases afterwards. This is due to an increase in bond length between Mo and S atoms which reduces the charge transfer when K_{eff} is larger than K_{flat}, which is seen in the form of decreasing E^{q-z}. Specifically, the charges on a Mo atom at K_{flat} and $1.4 \times K_{\text{flat}}$ are $0.55e$ and $0.43e$, respectively, which leads to a reduction in E^{q-z}. A simultaneous decrease in E^{p-z} is also observed due to an increase in the angle B-A-C, which increases from about $3.96°$ from K_{flat} to $1.4 \times K_{\text{flat}}$. Although the slope of the polarization P^z variation with K_{eff} is similar to the flexoelectric coefficient obtained in the case of bending towards the spontaneous curling direction, more energy is required to deform towards the Te layer in MoSTe as compared to the S layer in MoSTe. As a result, bending towards the S layer in MoSTe is a better choice for energy
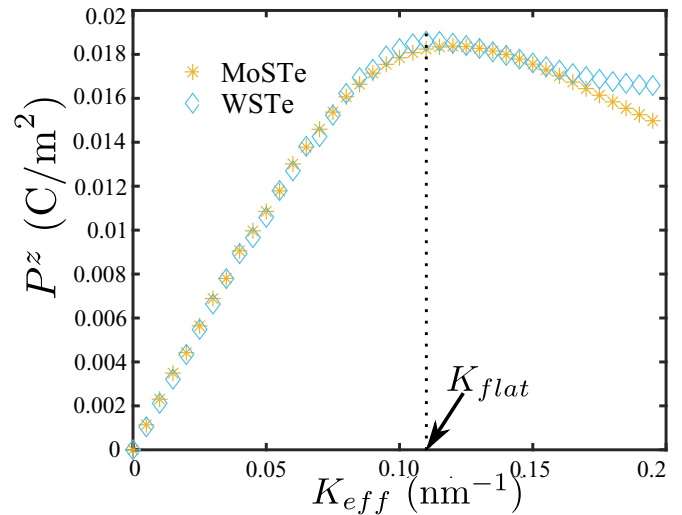

FIG. 4. The variation of polarization P^z with the effective strain gradient K_{eff} for MoSTe and WSTe when bending against their initial spontaneous curvature.

conversion. A similar observation is found in the case of WSTe.

IV. CONCLUSION

We have utilized classical molecular dynamics coupled with a charge-dipole model to study the bending flexoelectric response of Janus TMDCs. We further employed a prescribed bending deformation that enabled us to directly calculate the flexoelectric constants while eliminating the piezoelectric contribution to the polarization. In doing so, we found that Janus TMDCs have flexoelectric constants that are several times larger than traditional TMDCs, such as MoS$_2$. The mechanism underlying this was found to be bond length asymmetry for the Janus TMDCs between the M-X and the M-Y atoms. This bond length asymmetry was found to lead to stronger σ-σ interactions with increasing initial asymmetry along with stronger π-σ interactions due to increased charge transfer, which combine to result in increased polarization for Janus TMDCs.

The present results also demonstrate the enhanced electromechanical coupling that results from out-of-plane bending as compared to in-plane stretching for Janus TMDCs. Specifically, by comparing equivalent states of strain energy density, we found that the electrical energy density is higher for Janus TMDCs as compared to MoS$_2$, whereas the electrical energy density under tension is smaller than that of bending for Janus TMDCs. These facts imply that there may be benefits in electromechanical energy conversion for Janus TMDCs by utilizing out-of-plane bending flexoelectricity as compared to in-plane piezoelectricity.

[1] E. Pop, V. Varshney, and A. K. Roy, MRS Bull. **37**, 1273 (2012).

[2] S. Ghosh, W. Bao, D. L. Nika, S. Subrina, E. P. Pokatilov, C. N. Lau, and A. A. Balandin, Nature Mater. **9**, 555 (2010).

[3] R. Fei and L. Yang, Nano Lett. **14**, 2884 (2014).

[4] S. Yu, X. Wu, Y. Wang, X. Guo, and L. Tong, Adv. Mater. **29**, 1606128 (2017).

[5] Q. H. Wang, K. Kalantar-Zadeh, A. Kis, J. N. Coleman, and M. S. Strano, Nat. Nanotechnol. **7**, 699 (2012).

[6] P. Z. Hanakata, A. Carvalho, D. K. Campbell, and H. S. Park, Phys. Rev. B **94**, 035304 (2016).

[7] R. C. Andrew, R. E. Mapasha, A. M. Ukpong, and N. Chetty, Phys. Rev. B **85**, 125428 (2012).

[8] B. Javvaji, P. Budarapu, V. Sutrakar, D. R. Mahapatra, M. Paggi, G. Zi, and T. Rabczuk, Comput. Mater. Sci. **125**, 319 (2016).

[9] S. J. Kim, K. Choi, B. Lee, Y. Kim, and B. H. Hong, Annu. Rev. Mater. Res. **45**, 63 (2015).

[10] Z. Sun, A. Martinez, and F. Wang, Nat. Photonics **10**, 227 (2016).

[11] R. Mas-Ballesté, C. Gómez-Navarro, J. Gómez-Herrero, and F. Zamora, Nanoscale **3**, 20 (2011).

[12] X. Wang, H. Tian, W. Xie, Y. Shu, W.-T. Mi, M. A. Mohammad, Q.-Y. Xie, Y. Wang, J.-B. Xu, and T.-L. Ren, NPG Asia Mater. **7**, e154 (2015).

[13] X. Song, F. Hui, T. Knobloch, B. Wang, Z. Fan, T. Grasser, X. Jing, Y. Shi, and M. Lanza, Appl. Phys. Lett. **111**, 083107 (2017).

[14] X.-Q. Zheng, J. Lee, and P. X.-L. Feng, Microsyst. Nanoeng. **3**, 17038 (2017).

[15] M. Zelisko, Y. Hanlumyuang, S. Yang, Y. Liu, C. Lei, J. Li, P. M. Ajayan, and P. Sharma, Nat. Commun. **5**, 4284 (2014).

[16] M. N. Blonsky, H. L. Zhuang, A. K. Singh, and R. G. Hennig, ACS Nano **9**, 9885 (2015).

[17] S. I. Kundalwal, S. A. Meguid, and G. J. Weng, Carbon **117**, 462 (2017).

[18] S. Chandratre and P. Sharma, Appl. Phys. Lett. **100**, 023114 (2012).

[19] K.-A. N. Duerloo and E. J. Reed, Nano Lett. **13**, 1681 (2013).

[20] J. Zhang, Nano Energy **41**, 460 (2017).

[21] Y. Zhou, W. Liu, X. Huang, A. Zhang, Y. Zhang, and Z. L. Wang, Nano Res. **9**, 800 (2016).

[22] B. Javvaji, B. He, and X. Zhuang, Nanotechnology **29**, 225702 (2018).

[23] W. Wu, L. Wang, Y. Li, F. Zhang, L. Lin, S. Niu, D. Chenet, X. Zhang, Y. Hao, T. F. Heinz *et al.*, Nature (London) **514**, 470 (2014).

[24] K.-A. N. Duerloo, M. T. Ong, and E. J. Reed, J. Phys. Chem. Lett. **3**, 2871 (2012).

[25] C. J. Brennan, R. Ghosh, K. Koul, S. K. Banerjee, N. Lu, and E. T. Yu, Nano Lett. **17**, 5464 (2017).

[26] M. S. Majdoub, P. Sharma, and T. Cagin, Phys. Rev. B **77**, 125424 (2008).

[27] B. He, B. Javvaji, and X. Zhuang, Physica B **545**, 527 (2018).

[28] S. V. Kalinin and V. Meunier, Phys. Rev. B **77**, 033403 (2008).

[29] T. Dumitrică, C. M. Landis, and B. I. Yakobson, Chem. Phys. Lett. **360**, 182 (2002).

[30] X. Zhuang, B. He, B. Javvaji, and H. S. Park, Phys. Rev. B **99**, 054105 (2019).

[31] J. Wang, H. Shu, T. Zhao, P. Liang, N. Wang, D. Cao, and X. Chen, Phys. Chem. Chem. Phys. **20**, 18571 (2018).

[32] S. D. Guo, Phys. Chem. Chem. Phys. **20**, 7236 (2018).

[33] H. Jin, T. Wang, Z. R. Gong, C. Long, and Y. Dai, Nanoscale **10**, 19310 (2018).

[34] W. Shi and Z. Wang, J. Phys.: Condens. Matter **30**, 215301 (2018).

[35] H. Liu, Z. Huang, C. He, Y. Wu, L. Xue, C. Tang, X. Qi, and J. Zhong, J. Appl. Phys. **125**, 082516 (2019).

[36] R. Li, Y. Cheng, and W. Huang, Small **14**, 1802091 (2018).

[37] L. Dong, J. Lou, and V. B. Shenoy, ACS Nano **11**, 8242 (2017).

[38] A. Y. Lu, H. Zhu, J. Xiao, C. P. Chuu, Y. Han, M. H. Chiu, C. C. Cheng, C. W. Yang, K. H. Wei, Y. Yang, Y. Wang, D. Sokaras, D. Nordlund, P. Yang, D. A. Muller, M. Y. Chou, X. Zhang, and L. J. Li, Nat. Nanotechnol. **12**, 744 (2017).

[39] C. Zhang, Y. Nie, S. Sanvito, and A. Du, Nano Lett. **19**, 1366 (2019).

[40] L. Hu and X. Huang, RSC Adv. **7**, 55034 (2017).

[41] J. W. Jiang, Z. Qi, H. S. Park, and T. Rabczuk, Nanotechnology **24**, 435705 (2013).

[42] H. J. Jin, W. Y. Yoon, and W. Jo, ACS Appl. Mater. Interfaces **10**, 1334 (2018).

[43] S. Kang, S. Jeon, S. Kim, D. Seol, H. Yang, J. Lee, and Y. Kim, ACS Appl. Mater. Interfaces **10**, 27424 (2018).

[44] S. Kang, S. Kim, S. Jeon, W. S. Jang, D. Seol, Y. M. Kim, J. Lee, H. Yang, and Y. Kim, Nano Energy **58**, 57 (2019).

[45] A. Abdollahi, N. Domingo, I. Arias, and G. Catalan, Nat. Commun. **10**, 1266 (2019).

[46] S. Zhang, K. Liu, T. Wu, M. Xu, and S. Shen, J. Appl. Phys. **122**, 144103 (2017).

[47] W. Shi, Y. Guo, Z. Zhang, and W. Guo, J. Phys. Chem. Lett. **9**, 6841 (2018).

[48] A. Mayer, P. Lambin, and R. Langlet, Appl. Phys. Lett. **89**, 063117 (2006).

[49] A. Mayer, Phys. Rev. B **75**, 045407 (2007).

[50] J.-W. Jiang, Acta Mechanica Solida Sinica **32**, 17 (2019).

[51] Q.-l. Xiong, J. Zhou, J. Zhang, T. Kitamura, and Z.-h. Li, Phys. Chem. Chem. Phys. **20**, 20988 (2018).

[52] R. Kuate Defo, S. Fang, S. N. Shirodkar, G. A. Tritsaris, A. Dimoulas, and E. Kaxiras, Phys. Rev. B **94**, 155310 (2016).

[53] T. Hu, F. Jia, G. Zhao, J. Wu, A. Stroppa, and W. Ren, Phys. Rev. B **97**, 235404 (2018).

[54] C. Xia, W. Xiong, J. Du, T. Wang, Y. Peng, and J. Li, Phys. Rev. B **98**, 165424 (2018).

[55] F. Li, W. Wei, P. Zhao, B. Huang, and Y. Dai, J. Phys. Chem. Lett. **8**, 5959 (2017).

[56] Y. Ji, M. Yang, H. Lin, T. Hou, L. Wang, Y. Li, and S.-T. Lee, J. Phys. Chem. C **122**, 3123 (2018).

[57] S. Plimpton, J. Comput. Phys. **117**, 1 (1995).

[58] M. J. Frisch, G. W. Trucks, H. B. Schlegel, G. E. Scuseria, M. A. Robb, J. R. Cheeseman, G. Scalmani, V. Barone, G. A. Petersson, H. Nakatsuji, X. Li, M. Caricato, A. V. Marenich, J. Bloino, B. G. Janesko, R. Gomperts, B. Mennucci, H. P. Hratchian, J. V. Ortiz, A. F. Izmaylov, J. L. Sonnenberg, D. Williams-Young, F. Ding, F. Lipparini, F. Egidi, J. Goings, B. Peng, A. Petrone, T. Henderson, D. Ranasinghe, V. G. Zakrzewski, J. Gao, N. Rega, G. Zheng, W. Liang, M. Hada, M. Ehara, K. Toyota, R. Fukuda, J. Hasegawa, M. Ishida, T. Nakajima, Y. Honda, O. Kitao, H. Nakai, T. Vreven, K. Throssell, J. A. Montgomery, Jr., J. E. Peralta, F. Ogliaro, M. J. Bearpark, J. J. Heyd, E. N. Brothers, K. N. Kudin, V. N. Staroverov, T. A. Keith, R. Kobayashi, J. Normand,

K. Raghavachari, A. P. Rendell, J. C. Burant, S. S. Iyengar, J. Tomasi, M. Cossi, J. M. Millam, M. Klene, C. Adamo, R. Cammi, J. W. Ochterski, R. L. Martin, K. Morokuma, O. Farkas, J. B. Foresman, and D. J. Fox, GAUSSIAN 16 Revision B.01 (Gaussian Inc., Wallingford CT, 2016).

[59] A. Stukowski, Modell. Simul. Mater. Sci. Eng. **18**, 015012 (2009).

[60] M. L. Falk and J. S. Langer, Phys. Rev. E **57**, 7192 (1998).

[61] F. Shimizu, S. Ogata, and J. Li, Mater. Trans. **48**, 2923 (2007).

[62] F. Fabbri, E. Rotunno, E. Cinquanta, D. Campi, E. Bonnini, D. Kaplan, L. Lazzarini, M. Bernasconi, C. Ferrari, M. Longo, G. Nicotra, A. Molle, V. Swaminathan, and G. Salviati, Nat. Commun. **7**, 13044 (2016).

[63] R. Gleiter, Pure Appl. Chem. **59**, 1585 (1987).

[64] V. J. Surya, K. Iyakutti, H. Mizuseki, and Y. Kawazoe, Comput. Mater. Sci. **65**, 144 (2012).

[65] I. Nikiforov, E. Dontsova, R. D. James, and T. Dumitrică, Phys. Rev. B **89**, 155437 (2014).

[66] N. A. Pike, B. Van Troeye, A. Dewandre, G. Petretto, X. Gonze, G. M. Rignanese, and M. J. Verstraete, Phys. Rev. B **95**, 201106(R) (2017).

[67] D. Er, H. Ye, N. C. Frey, H. Kumar, J. Lou, and V. B. Shenoy, Nano Lett. **18**, 3943 (2018).

[68] L. Pan, B. Zou, and L. J. Shi, Phys. Lett. A **380**, 2227 (2016).

[69] P. V. Yudin and A. K. Tagantsev, Nanotechnology **24**, 432001 (2013).

[70] P. Zubko, G. Catalan, and A. K. Tagantsev, Annu. Rev. Mater. Res. **43**, 387 (2013).